Nodal Cilia Dynamics and the Specification of the Left/Right Axis in Early Vertebrate Embryo Development

Javier Buceta,* Marta Ibañes,† Diego Rasskin-Gutman,† Yasushi Okada,‡ Nobutaka Hirokawa,‡
and Juan Carlos Izpisúa-Belmonte†
*Centre de Recerca en Química Teòrica (CeRQT), Parc Científic de Barcelona, Campus Diagonal-Universitat de Barcelona, Edifici Modular, Barcelona, Spain; †Gene Expression Laboratory, The Salk Institute for Biological Studies, La Jolla, California; and ‡Department of Cell Biology & Anatomy, University of Tokyo, Graduate School of Medicine, Tokyo, Japan

ABSTRACT Nodal cilia dynamics is a key factor for left/right axis determination in mouse embryos through the induction of a leftward fluid flow. So far it has not been clearly established how such dynamics is able to induce the asymmetric leftward flow within the node. Herein we propose that an asymmetric two-phase nonplanar beating cilia dynamics that involves the bending of the ciliar axoneme is responsible for the leftward fluid flow. We support our proposal with a host of hydrodynamic arguments, in silico experiments and in vivo video microscopy data in wild-type embryos and *inv* mutants. Our phenomenological modeling approach underscores how the asymmetry and speed of the flow depends on different relevant parameters. In addition, we discuss how the combination of internal and external mechanisms might cause the two-phase beating cilia dynamics.

INTRODUCTION

During vertebrate embryo development three spatial body axes are specified (1). The specification of the left/right (L/R) axis prompts Nature to perform a chiral choice, posing the interesting question of how it manages to make the same choice systematically. In recent years a number of reports have connected the presence of monociliated cells in the node of mouse embryos with early L/R axis specification (2–5). These nodal cells exhibit cilia with 9+0 architecture that apparently rotate in a clockwise direction (ventral view). In wild-type (*wt*) phenotypes such motion collectively generates a fast asymmetric leftward fluid flow within the node. Accordingly, mutant mouse embryos either lacking cilia or with immotile cilia in the node show L/R randomization as well as absence of directional fluid flow (2–3,6–7). In addition, elegant experiments have shown that the phenotype in mutant embryos with immotile cilia can be rescued if an external artificial fast leftward flow is imposed (8). Moreover, by applying an artificial rightward fluid flow inside the node of *wt* embryos, the correct positioning of organs (situs) is reversed (8). These experimental evidences highlight the importance of nodal cilia dynamics to induce an asymmetric flow that subsequently establishes the proper situs in mouse embryos. Importantly, recent experiments have shown that such leftward fluid flow dynamics is conserved among different species (5,9).

Two mechanisms have been proposed to explain the role of fluid flow in specifying the phenotypes and gene expression patterns of *wt* and mutant embryos: the advection by the fluid flow of a protein (morphogen) toward the left side of the node, and the bending of mechanosensor immotile cilia (2,3,5,10,11). Independently of which of these two mechanisms, or combination of them, is responsible for the subsequent asymmetric gene expression cascade, the aforementioned evidences indicate that the dynamics of the nodal fluid flow constitutes a crucial step of the L/R symmetry breaking process. In this regard, several open questions remain. Herein we address a number of them. First, how the motion of the cilia leads to an asymmetric leftward flow. Second, how the ciliary dynamics coordinates the two symmetries previously broken to specify the L/R axis systematically. Third, what the elements are that lead to an anomalous fluid flow dynamics in the so-called *inv* mutants.

Theoretical models in L/R specification have been advanced at many levels, including reaction diffusion systems, regulatory networks, or cooperative adhesive dynamics (12–14). Also, the dynamics of cilia and flagella have been modeled and simulated at various degrees of detail (15–18). Specifically, Brokaw has recently analyzed the mechanism by which nodal cilia rotate clockwise in the *wt* murine node (19). However, only Cartwright and collaborators have recently explored the fluid flow of the murine node, albeit their modeling approach did not involve a detailed characterization of the structure and dynamics of the cilia. Still, they correctly predicted that nodal cilia move around an axis tilted to the posterior in the *wt* (20,5).

The nodal fluid flow regime corresponds to low Reynolds numbers (LRN) where motion follows Aristotelian dynamics rather than Newtonian dynamics. The Reynolds number, *Re*, measures the importance of the inertial forces with respect to the viscous forces in a fluid flow: $Re = L_c U/\upsilon$, where L_c is a characteristic length, U is a characteristic velocity, and υ is the kinematic viscosity. In the case of the murine node, if we take L_c to be the width of the node (50 μm), U as the leftward

---

Submitted March 29, 2005, and accepted for publication June 16, 2005.

Javier Buceta, Marta Ibañes, and Diego Rasskin-Gutman contributed equally to this work.

Address reprint requests and inquiries to J. Buceta, E-mail: jbuceta@pcb.ub.es or J. C. Izpisúa-Belmonte, E-mail: belmonte@salk.edu.

© 2005 by the Biophysical Society

0006-3495/05/10/2199/11 $2.00

doi: 10.1529/biophysj.105.063743

flow speed (5–50 μm/s), and υ as the kinematic viscosity of an aqueous medium, $\upsilon = 10^{-6}$ m^2/s, the Reynolds number is of order 10^{-3}, indicating that viscosity dominates over inertia (20). It has been established that, due to the lack of inertia in this regime, and disregarding possible boundary effects, at least two degrees of freedom are needed to induce a directional motion, which is commonly known as the Scallop Theorem (21). Thus, a rotating stiff cilium can hardly generate an asymmetric flow in the LRN regime. Indeed Cartwright and collaborators proposed that posteriorly tilted rotating cilia (modeled by means of rotlets) induce a leftward flow above the rotlets (20). However, they also point out that in the absence of boundary conditions an equally fast rightward flow is induced below the rotlets. Therefore additional elements are required to explain the emergence of an asymmetric directional leftward fluid flow. Some authors have claimed that the shape of the ciliated organ, i.e., the boundary conditions, might be crucial to determine the asymmetric flow (2,3,22). However, previous theoretical studies (20) and recent experimental results (5) have shown otherwise. It has also been proposed that the presence of cell surfaces creates a viscous resistance that slows down the flow induced by tilted cilia motion (20,23). However, the presence of the cell surface alone does not ensure that the flow will still be leftward close to the cell surface (and not rightward but slow), as experimentally measured (5,20,23).

Directional fluid motion has been thoroughly studied in the context of 9+2 cilia and flagella, which show a characteristic two-phase beating dynamics, with a power and recovery stroke that is predominantly planar, i.e., their phases of motion occur in the same plane. This two-phase dynamics induces a unidirectional fluid flow in the direction of the power stroke (23,24). Primary cilia with a 9+0 architecture are mostly immotile mechanosensors widely found in the surface of many cells both in embryos and adults of many species (25). In the case of the embryo node, the primary cilia are a notable exception and show, as mentioned above, an apparent rotational motion. Some flagella, such as the eel sperm flagellum, also show a 9+0 architecture and do move. In this case, their motion is nonplanar describing an helicoidal waveform (26). Furthermore, experiments with mutant *Chlamydomonas* showing a 9+0 phenotype in their flagella instead of their normal 9+2 structure (27) confirm that whereas the 9+2 flagella have a planar beating motion, mutant flagella lacking the central-pair of microtubules perform a more irregular asymmetric beating motion when demembranated and in the presence of low calcium concentration ($<10^{-6}$ M). Thus, planar and three-dimensional beating patterns seem to be interchangeable given the right external conditions, such as concentration of calcium and viscosity (28). In the case of nodal cilia, the absence of the central pair of microtubules in the 9+0 cilia might prevent planar motion altogether (29).

Taking into account all these evidences, we asked whether the motion reported for nodal cilia could correspond to a more complex movement pattern than the one reported so far. Thus, we propose that the apparent rotational motion of cilia actually corresponds to a two-phase nonplanar beating dynamics. We analyze this claim by providing in silico experiments that are supported by in vivo data. To investigate the flow induced by such collective ciliary activity we use a ''simple'' hydrodynamics modeling approach. Within this framework we keep the minimum, yet sufficient, level of detail to account for the ciliary dynamics in a realistic manner. Our approach shows that a two-phase nonplanar beating dynamics is able to induce an asymmetric leftward flow. The underlying mechanism rests on the idea that such motion results from 1), the combined action of internal active motors that produce the bending of the ciliary axoneme and the two-phase dynamics typical of cilia and flagella; and 2), the external viscous interaction between the cilia and the fluid flow when wall effects due to the cell surfaces are taken into account. Moreover, these results are in agreement with recent experiments on nodal monocilia, which suggest that such dynamics is crucial for establishing an asymmetric leftward flow that is conserved among different species (5).

MATERIALS AND METHODS

In silico experiments: numerical simulations

We have adimensionalized the equation of motion for the bead such that the unity length corresponds to twice the length of mouse nodal cilia ($L = 5$ μm), and the angular frequency of rotation during the effective stroke is set to $\omega = 1$. The differential equations have been integrated using a fourth-order Runge-Kutta algorithm. The average speed $\langle \vec{u} \rangle$ of beads embedded in the nodal flow has been computed from the speed of 81 beads moving in the nodal region during 15 periods of rotation. The beads are distributed uniformly in a plane $z = 5$ μm above the cell surfaces and embedded in the flow created by 36 cilia forming a square. The standard deviation σ is obtained from the average speed of each bead. There are no significant differences between the average flow on a square or a pearshaped configuration of cilia. In addition, the average flow for *inv* mutants has been computed over five different arrangements of cilia.

In vivo experiments: video-microscopy details

The embryos of timed pregnant ICR mice (CLEA Japan, Meguro-ku, Tokyo, Japan) were dissected and mounted on a silane-coated glass slide with a silicone-rubber spacer, as described previously (3). Only embryos with a fully developed node (nodal stage *5* or *6*) were selected for the analysis (3). For high-speed recording of the ciliary activity, the differential interference contrast image technique was employed. High-speed recording was implemented by a CCD camera, HG Imager 2000 (Eastman Kodak, Rochester, NY), at 500 frames/s (see Supplementary Material, Movies S1 and S2). The genotype of mutant mouse embryos was determined after observation (3).

The digitized images of the high-speed CCD camera were analyzed with NIH Image software (free software developed at the National Institutes of Health). The tip and root of each cilium were traced in each video frame. The rotational axis was estimated fitting the projected trajectory of the tip of a cilium (ventral view projection) with an ellipse. We assumed a circular shape for the nonprojected trajectory. Our results indicate that cilia move around an axis tilted 40° ± 10° to the posterior with an apical angle of 40°. We estimated the angular frequency by back-projecting the trace of the tip to the plane perpendicular to the rotational axis of rotation. For a stiff cilium rotating at constant angular speed, such frequency should lead to a constant value. In contrast, we obtain that the frequency varies as a function of time (Fig. 6, *c* and *d*) and has two distinct phases: power stroke (fast motion) and recovery stroke (slow motion). The average frequency of rotation is 10 Hz, as previously reported. The same calculation for an in silico cilium gives similar qualitative results. We estimate the phenomenological elastic relaxation time, τ_b, by means of the ratio between the angular speed during the recovery stroke and the power stroke. For a detailed description of the analysis of in vivo experimental data, see Okada et al. (5).

Cilia bending

The local bending introduced by means of our modeling framework can be readily obtained. This gives an estimate of the actual bending of nodal cilia. Without lost of generality in regard to the following calculation, we assume a coordinate system for which $\Theta = 0°$ and $\theta = 0°$. First, note that $\vec{R}_{i+1,k}(t) = \vec{R}_{i,k}(t) + \vec{e}_{i+1,k}(t)$, where $\vec{e}_{i+1,k}(t) = (L/n)\,(\sin\Psi \sin\beta_{i+1}(t), \sin\Psi\cos\beta_{i+1}(t), \cos\Psi)$. Thus, the local bending between three consecutive spheres reads $\lambda = |\vec{e}_{i+1,k}(t)|\sin\phi = 2a\sin\phi$, where ϕ is the angle defined between $\vec{e}_{i+1,k}(t)$ and $\vec{e}_{i,k}(t)$ (Fig. 2 *a*). Such an angle can be computed in terms of the scalar product, $\vec{e}_{i+1,k}(t)\cdot\vec{e}_{i,k}(t) = (L^2/n^2)\cos\phi = (L^2/n^2)$ $(\sin^2\psi\,(\sin\beta_{i+1}\sin\beta_i + \cos\beta_{i+1}\cos\beta_i) + \cos^2\psi)$. We now notice that the maximal angular deflection between three consecutive spheres, $\Delta\beta$, is $\Delta\beta = \tau_b\omega/(n-1) \approx 5\cdot 10^{-2}\pi$ (Fig. 1 *b*). During the time span this maximal difference lasts, the relation $\beta_{i+1} = \beta_i + \Delta\beta$ holds and it is easy to check that the product $\vec{e}_{i+1,k}(t)\cdot\vec{e}_{i,k}(t)$ becomes β_i-independent: $\vec{e}_{i+1,k}(t)\cdot\vec{e}_{i,k}(t) = (L^2/n^2)\cos\phi = (L^2/n^2)\,(\sin^2\psi\cos\Delta\beta + \cos^2\psi)$. Thus, $\lambda = 2a\sin\phi = 2a\sqrt{1-(\sin^2\psi\cos\Delta\beta+\cos^2\psi)^2}$, and as expected, no bending is obtained if $\Delta\beta = 0$ ($\tau_b = 0$). An upperbound of the total bending of the cilium can be estimated as $\Lambda = n\lambda = L\sqrt{1-(\sin^2\psi\cos\Delta\beta+\cos^2\psi)^2} \approx 0.1\,\mu m$. This value is greater than the bending elicited by the viscous drag.

MODELING APPROACH FOR CILIA DYNAMICS

The motion of 9+2 beating cilia has been described as a two-phase dynamics with an effective or power stroke and a recovery stroke (23). The power stroke occurs while the extended cilium moves rapidly and far from the cell surface. The recovery stroke corresponds with the return of the bent cilium, with slower motion close to the cell surface (23). We interpret the motion of the 9+0 nodal cilia as similar nonplanar two-phase beating dynamics. Indeed, high-resolution in vivo video-microscopy data depict a two-phase motion with slow and fast strokes of the cilium and the bending of the cilia when moving more slowly close to the cell surface (Supplementary Material, Movies S1 and S2; Fig. 6 *d*; Materials and Methods; see also Okada et al. (5)). In addition, these experimental data support the theoretical proposal by Cartwright and colleagues that cilia move around an axis tilted to the posterior (20).

To account for a two-phase beating ciliary dynamics that includes bending we use the formalism of polymer hydrodynamics (30). This approach allows a realistic description of cilia by taking into account their length, width, and flexibility. Then, we model each cilium as a string of *n* moving spheres of radius *a* connected by massless rods plus one static sphere at the base (Fig. 1 *a*). The model can be applied to any cilia by setting the correct parameter values. For mouse embryos, the radius of a nodal cilium is $a \approx 150$ nm and its length is $L \approx 5\ \mu$m, and therefore $n = (L-a)/2a \approx 16$.

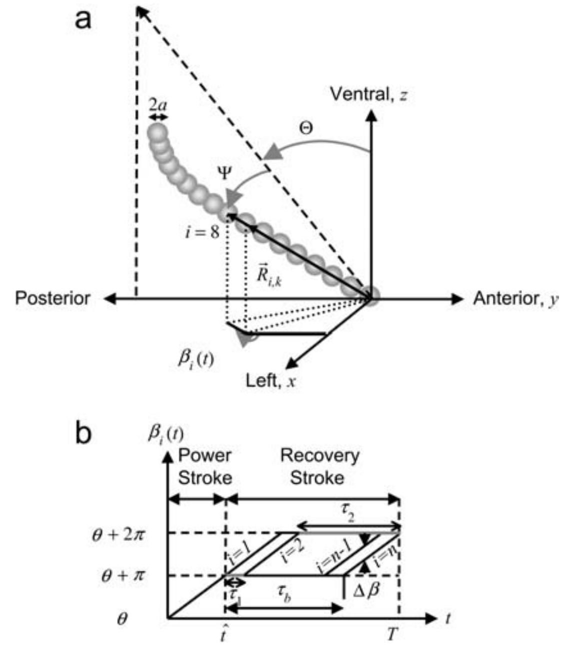

FIGURE 1 (*Top*) Cilia are modeled as strings of spheres. For mouse embryos, the radius and length of cilia are $a \approx 150$ nm and $L \approx 5\ \mu$m, respectively (~16 moving spheres). The average frequency of rotation is 10 Hz. Θ, Ψ, and β stand for the tilting, apical, and rotational angles, respectively. (*Bottom*) Time-evolution of the angular variable $\beta_i(t)$ during one period of beating. The function $\beta_i(t)$ characterizes the nonplanar beating dynamics as well as the bending of the cilium along its length. Since the cilium is flexible and can bend, $\beta_i(t)$ changes along the cilium's length. During each rotation, the cilium undergoes a two-phase motion corresponding to the effective and recovery strokes. The elastic relaxation time $\tau_b = \tau_1 + \tau_2$ accounts for the time-dependent bending of the cilium. The parameters τ_1 and τ_2 of sphere 2 are indicated. The maximal angular deflection between three consecutive spheres, $\Delta\beta$, has been indicated.

For a cilium that is moving around an axis tilted with angle Θ in the anteroposterior direction, the vector position $\vec{R}_{i,k}(t) = (x_{i,k}(t), y_{i,k}(t), z_{i,k}(t))$ of sphere *i* of cilium *k* reads (Fig. 1)

$$\begin{aligned}
x_{i,k}(t) &= \frac{L}{n}\sin\Psi\sum_{j=1}^{i}\sin\beta_j(t) + x_{0,k}\\
y_{i,k}(t) &= \frac{L}{n}\left[-i\sin\Theta\cos\Psi + \cos\Theta\sin\Psi\sum_{j=1}^{i}\cos\beta_j(t)\right] + y_{0,k}\\
z_{i,k}(t) &= \frac{L}{n}\left[i\cos\Theta\cos\Psi + \sin\Theta\sin\Psi\sum_{j=1}^{i}\cos\beta_j(t)\right] + z_{0,k},
\end{aligned} \tag{1}$$

where we have assumed, supported by the experimental observations (5), that Ψ and Θ are constants ($\Psi \approx 40°$ and $\Theta \approx 40°$) for all *i*. Note that at any given time $|\vec{R}_{i,k}(t) - \vec{R}_{i-1,k}(t)| = L/n$, so that the length of the cilium is time-invariant. Therefore, as noted in Eq. 1, all the ciliary dynamics is contained in the rotational functions $\beta_i(t)$ (Fig. 1). If cilia were rigid rods, their dynamics would be described by simply setting $\beta_i(t) = \omega t + \theta$, where ω is the angular velocity and θ is an arbitrary phase. However, for a two-phase beating dynamics involving ciliary bending a more elaborated definition is required. We account for such a two-phase dynamics by means of a phenomenological approach: during the power stroke, the cilium is extended and traces half of the trajectory with angular velocity $\dot{\xi}_{\text{pow}} = \omega$; during the recovery stroke, the cilium bends (Materials and Methods) and completes the cycle with a reduced average angular speed $\dot{\xi}_{\text{rec}} = \omega/(1 + \omega\tau_{\text{b}}/\pi)$. Note that we have introduced a phenomenological elastic relaxation time constant, τ_{b}. As mentioned above, video-microscopy images indeed reveal that cilia are performing a two-phase dynamics (see Supplementary Material, Movies S1 and S2; Fig. 6 *d*, and Okada et al. (5)) with a ratio between recovery and power stroke ($\dot{\xi}_{\text{rec}}/\dot{\xi}_{\text{pow}} \approx 0.6 - 0.7$) that fixes the elastic relaxation time $\tau_{\text{b}}\omega \approx 0.5\pi$ (Materials and Methods). From the modeling point of view, such timescale leads to a time-delayed dynamics for the rotational functions $\beta_{\text{i}}(t)$ as follows. We begin by defining the functions,

$$\begin{aligned}
\chi_1(t) &= H(t\,\text{mod}(T))\,H(\hat{t} - t\,\text{mod}(T)),\\
\chi_2(t) &= H(t\,\text{mod}(T) - \hat{t})\,H(\hat{t} + \tau_1 - t\,\text{mod}(T)),\\
\chi_3(t) &= H(t\,\text{mod}(T) - \hat{t} - \tau_1)\,H(2\hat{t} + \tau_1 - t\,\text{mod}(T)),
\end{aligned}$$

where $H(x)$ is the Heaviside function, $\hat{t} = \pi/\omega$ is the time the power stroke lasts, and $T = 2\hat{t} + \tau_{\text{b}}$ is the total period of motion. Thus, the average frequency is $f = 1/T$, which for mouse embryos takes the value $f \approx 10$ Hz. The functions $\chi_{\text{i}}(t)$ section the time-interval into periodic pieces of length T. Those pieces are partitioned into $(0, \hat{t}), (\hat{t}, \hat{t} + \tau_1), (\hat{t} + \tau_1, 2\hat{t} + \tau_1)$, and $(2\hat{t} + \tau_1, T)$. We also define the following piecewise periodic function, $b(t,\tau_1,\tau_2) = \omega t \text{ mod}(T)\ \chi_1(t) + \pi\chi_2(t) + \omega(t - \tau_1) \text{ mod}(T)\ \chi_3(t) + \theta$, where $\tau_{\text{b}} = \tau_1 + \tau_2$. The parameter θ characterizes the direction with respect to the motion of the cilium when performing the power and the recovery strokes. In the case of a clockwise motion, if $\theta = \pi/2$ ($\theta = 3\pi/2$), the cilium acts as a straight rod, power stroke, when rotating toward the right (left) and it bends, recovery stroke, when moving toward the left (right). For nodal cilia, which are tilted to the posterior, we set $\theta = 3\pi/2$ and thus, the recovery stroke occurs when the cilium moves close to the cell surface. With these definitions, the two-phase motion of cilia can finally be represented by setting

$$\beta_{\text{i}}(t) = b\left(t, \frac{(i-1)\tau_{\text{b}}}{(n-1)}, \frac{(n-i)\tau_{\text{b}}}{(n-1)}\right), \tag{2}$$

where the time delay satisfies $\pi(n - 1)/\omega > \tau_{\text{b}} > 0$. Fig. 1 shows the function $\beta_{\text{i}}(t)$ during one beating cycle. Note that, during the power stroke, the cilium advances as a straight rod and all spheres move together for a time $\hat{t}$. However, during the recovery stroke each sphere waits for a time τ_1 (sphere-dependent) before starting to move on its own. During this waiting time each sphere moves when pulled by other spheres (see Eq. 1). Then it starts moving again on its own for a time $\hat{t}$ before stopping again for a time $\tau_2 = \tau_{\text{b}} - \tau_1$, waiting until all spheres have completed the cycle and have returned to their initial positions. As a result the cilium bends (see Supplementary Material, Movies S1 and S2). We stress that if $\tau_{\text{b}} = 0$, the cilium does not bend and it induces symmetric leftward and rightward flows.

MECHANISMS FOR CILIA BEATING

The two-phase nonplanar beating motion of nodal cilia which involves bending of the ciliary axoneme and a slowing-down of the motion when sweeping close to the cell surface could be a result of internal driving mechanisms and/or external conditions. Biological motion in eukaryotic cells is usually accomplished by three ATP-consuming motors: myosins, kinesins, and dyneins (31,32). Axonemal dyneins drive the movement of cilia and flagella and their lack of function has been related to the Kartagener syndrome that produces situs inversus phenotypes (33,34). Moreover, bending of the 9+2 ciliary axoneme is known to be caused by an active sliding of microtubules orchestrated by dyneins (24,31) and we already mentioned that absence of the central microtubules prevents planar motion in 9+0 cilia (29,35). Therefore, we can hypothesize that the beating dynamics of nodal cilia is a result of an active internal mechanism involving the sliding activity of dynein. At present, it is not yet known how the directions of the two-phase beating cilia and flagella dynamics are established. Recently it has been shown that the sliding activity of dyneins depends itself on an externally imposed bending of the axoneme (36). Therefore, we could envisage the possibility that an external element to the cilium that favors ciliary bending along a specific direction can be driving the directions of the power and recovery strokes. The cell surface creates a viscous resistance such that the closer to it, the more difficult it is to move in the surrounding fluid (23). Thus, cilia moving around an axis tilted with respect to the cell surface's perpendicular direction encounter a higher viscous resistance in their phase of motion when moving closer to the cell surface. Thus, one might hypothesize that, as a result of this viscous interaction, the cilia bend. We now proceed to test this hypothesis. The stiffness of nodal cilia with respect to thermal forces can be estimated by means of the dimensionless ratio l_{p}/L, where l_{p} is the so-called persistence length (37,38). The latter accounts for the length beyond which the cost in terms of elastic energy for bending is negligible, $l_{\text{p}} = EI/KT$, where EI stands for the bending stiffness, K is the Boltzmann constant, and T is the temperature (~300 K). The stiffer the material, the larger the l_{p}. For microtubules and flagella EI has been estimated to be 10^{-23} Nm^2 and 10^{-22} Nm^2, respectively (39–41), that leads to the ratio $l_{\text{p}}/L \approx 10^4$, i.e., a rather stiff cilium to be bent by means of thermal fluctuations. This result allows us to effectively evaluate the elastic properties of cilia using a continuum approximation. Thus, a rough estimate of the bending induced by the drag can be obtained by treating cilia as cantilevered beams moving in a flow that exerts a force along the beam, F, parallel to the base plane where the beam is attached (42). The displacement of the free end with respect to an inflexible beam reads in that case, $\Lambda = FL^3/8EI$, where we note that possible twisting effects and the weight of the beam have not been considered. The force can be estimated by means of the approximated solution that accounts for the drag at LRN of a cylinder of radius a moving in a flow with relative velocity v_0 (43),

$$F = \frac{8\pi L v_0 \eta}{1 - 2\left[\gamma + ln\left(\frac{a v_0}{4\upsilon}\right)\right]}.$$

Taking into account that the nodal fluid is an aqueous medium, $\eta \approx 10^{-3}$ Ns/m^2, $\upsilon \approx 10^{-6}$ m^2/s, and that the relative velocity of the cilia to the flow is of order $v_0 \approx 10$ μm/s, the displacement induced by the drag becomes $\Lambda \approx 0.01$ μm. Our modeling framework permits us to estimate the bending involved in the cilia dynamics observed in experiments, and accordingly to analyze whether this bending is only due to the viscous drag. Such calculation indicates that the bending of nodal cilia is at most $\Lambda \approx 0.1$ μm (Materials and Methods). Thus, the drag does not account by itself for all the observed bending but contributes to it. Moreover, the experimental observations presented herein and in a recent work show that the slowing-down of the motion and the bending always occurs when the cilium is moving close to the cell surface: cilia tilted to the posterior/ anterior slow down and bend when moving rightward/ leftward (Fig. 6 *d*; see also Okada et al. (5). This result introduces a correlation between viscous forces (drag) and bending that suggests the importance of the former as the external mechanism that drives the ciliary dynamics.

According to all these evidences and our numerical analysis we propose that the bending of the ciliary axoneme might be due to a combination of internal and external mechanisms. Thus, we conjecture that the former would be responsible for the two-phase dynamics whereas the latter would be a guiding force. In this way, cilia would use the external mechanism of bending to instruct the internal machinery when performing each of the two phases of motion, such that the resistance to the medium is reduced when it is largest. Such phase resetting is achieved in our modeling approach by conveniently setting up the angular phase θ, depending on the value of Θ. By means of this orchestrated mechanism, an optimal performance from an energetic point of view would be obtained.

MODELING APPROACH FOR THE FLUID FLOW

The nodal fluid flow has been experimentally visualized by the motion of small latex fluorescent beads added to the embryo culture medium. Thus, to have a realistic comparison of our theoretical results with the experimental data, we have formulated the equations describing the dynamics of such beads embedded in the nodal fluid. The equation of motion for a small spherical particle in a nonuniform flow can be derived from first principles (44). An analysis of such an equation for LRN reveals that the beads used in the nodal experiments are truly passive tracers: their velocities in the bulk of the node correspond to the fluid velocity. Moreover, since in the LRN regime the Navier-Stokes equations describing the dynamics of the extraembryonic fluid become linear, the flow generated by an ensemble of cilia can be approximated as the sum of the flow induced by each single cilium. Temperature corrections are of second order, and the effect of the curvature or wall lift can be perceived only near the boundaries.

Thus, the equation of motion of a bead in the node simply reads

$$\frac{d\vec{r}}{dt} = \vec{u}(\vec{r}, t),$$

where $\vec{r}$ is the position of the bead and $\vec{u}(\vec{r}, t)$ the velocity field that at position $\vec{r}$ and time t is produced by the dynamics of the cilia. Thus, the velocity field $\vec{u}(\vec{r}, t)$ appears as a result of the action of the N cilia present within the node, each of which is modeled by means of $n + 1$ spheres, as previously described. That is,

$$\vec{u}(\vec{r}, t) = \sum_{\mathrm{k}=1}^{\mathrm{N}} \vec{u}_{\mathrm{k}}(\vec{r}, \{\vec{R}_{\mathrm{i,k}}\}, t),$$

where $\vec{u}_{\mathrm{k}}(\vec{r}, \{\vec{R}_{\mathrm{i,k}}\}, t)$ is the velocity field that at point $\vec{r}$ and time t is induced by the dynamics of cilium k that has its basis at $\vec{R}_{0,\mathrm{k}}$ and is formed by a set of n moving spheres with locations $\{\vec{R}_{\mathrm{i,k}}\}_{\mathrm{i}=1,\ldots,\mathrm{n}}$.

Once the dynamics of the spheres has been fixed (Eqs. 1 and 2), the velocity field $\vec{u}_{\mathrm{k}}(\vec{r}, \{\vec{R}_{\mathrm{i,k}}\}, t)$ induced by cilium k is computed in terms of the coordinates and velocities of the spheres that define the cilium by means of the well-known hydrodynamic expression that accounts for the velocity field induced by a moving sphere in a quiescent fluid (45). Specifically, $\vec{u}_{\mathrm{k}}(\vec{r}, \{\vec{R}_{\mathrm{i,k}}\}, t)$ is the sum of the velocity fields generated by the spheres of the cilium,

$$\begin{aligned}\vec{u}_{\mathrm{k}}(\vec{r}, \{\vec{R}_{\mathrm{i,k}}\}, t) = {} & \frac{3}{4}\sum_{\mathrm{i}=0}^{\mathrm{n}} \frac{a_{\mathrm{i,k}}(t)}{|\vec{r} - \vec{R}_{\mathrm{i,k}}|^3} \\ & \times \left[ ]\dot{\vec{R}}_{\mathrm{i,k}} \left(|\vec{r} - \vec{R}_{\mathrm{i,k}}|^2 + \frac{a^2_{\mathrm{i,k}}(t)}{3} \right) + (\vec{r} - \vec{R}_{\mathrm{i,k}}) \right. \\ & \left. \times \left((]\dot{\vec{R}}_{\mathrm{i,k}} \cdot (\vec{r} - \vec{R}_{\mathrm{i,k}})) \left(1 - \frac{a^2_{\mathrm{i,k}}(t)}{|\vec{r} - \vec{R}_{\mathrm{i,k}}|^2} \right) \right) \right].\end{aligned} \tag{3}$$

Let us briefly comment on some limitations, and advantages, introduced by our modeling approach. As noted in Eq. 3, each individual sphere moves in a quiescent fluid contributing independently (besides the local conformation effects indicated below) to generate the fluid flow. This disregards the hydrodynamic interactions between spheres that could be taken into account on the basis of the Oseen-Kirkwood theory (46). However, the problem becomes extraordinarily complicated from the analytical and computational points of view and yields, in regard of the main goal of this work, an unnecessary level of detail. Drawing parallels with related problems in polymer hydrodynamics, we have considered instead a simplification *à la* Rouse: a first-order approximation to the fluid velocity field where no hydrodynamic interaction between monomers is taken into account but which, significantly, allows us to qualitatively depict the polymeric dynamics (47). The advantage of our approximation may be readily foreseen: we keep the complexity of our simulation scheme at a minimum, but ensuring that the level of detail is enough to describe the ciliary activity in an effective manner and, more importantly, its effects.

Nonetheless, to capture the inherent effect caused by cilia bending into the fluid flow, conformational effects must be taken into account. Thus, the local conformation (or shape) of the cilium has been included in $\vec{u}_k(\vec{r}, \{\vec{R}_{i,k}\}, t)$ by means of time-dependent radii $a_{i,k}(t)$, to reflect the fact that moving an elongated object in the direction of its main (long) axis is easier than moving it in the direction perpendicular to its main axis (48). The velocity field generated by a moving sphere depends on the radius ''exposed'' to the surrounding fluid. Then, note that the local conformation of the cilium masks such radius since each sphere is attached to its neighboring spheres by massless rods with directions $\vec{e}_{i\pm1,k} = \vec{R}_{i\pm1,k} - \vec{R}_{i,k}$. We account for this fact by defining an effective radius in terms of the portion of the radius that is covered by neighboring spheres with respect to its direction of motion (Fig. 2 *b*). We compute the effective radius of each sphere as follows. Let us consider sphere i and its nearest neighbors $i + 1$ and $i - 1$. If sphere i from cilium k is moving with velocity $]\vec{R}_{i,k}$, the portion of its diameter that is *not* covered by a neighbor with respect to its direction of movement reads (Fig. 2 *b*)

$$|\vec{e}_{i\pm1,k}|\sin\alpha = \left|\frac{]\dot{\vec{R}}_{i,k}}{|]\dot{\vec{R}}_{i,k}|} \times \vec{e}_{i\pm1,k}\right|.$$

Therefore, the portion along the diameter of sphere i perpendicular to its speed that is covered by its neighboring spheres ($i + 1$ or $i - 1$) becomes

$$d_{i\pm1,k}(t) = \left(2a - \left|\frac{]\dot{\vec{R}}_{i,k}}{|]\dot{\vec{R}}_{i,k}|} \times \vec{e}_{i\pm1,k}\right|\right) H\left(\vec{e}_{i\pm1,k} \cdot \frac{]\dot{\vec{R}}_{i,k}}{|]\dot{\vec{R}}_{i,k}|}\right).$$

The Heaviside function indicates that only neighboring spheres located (with respect to the direction of motion of sphere i) in front of (and not behind) sphere i affect its drag. Thus, we define the effective radius of sphere i as

$$a_{i,k}(t) = \left[a - \frac{1}{2}(d_{i+1,k} + d_{i-1,k})\right] H\left(a - \frac{1}{2}(d_{i+1,k} + d_{i-1,k})\right).$$

The last term avoids negative radii arising when the angle between $\vec{e}_{i+1,k}$ and $\vec{e}_{i-1,k}$ is less than $\pi/2$ and $]\vec{R}_{i,k}$ lies between those vectors. A time-dependent bending that reduces the drag of the cilium and induces a slower flow during the recovery phase than during the power stroke is a mandatory component of the proposed mechanism as we will show below.

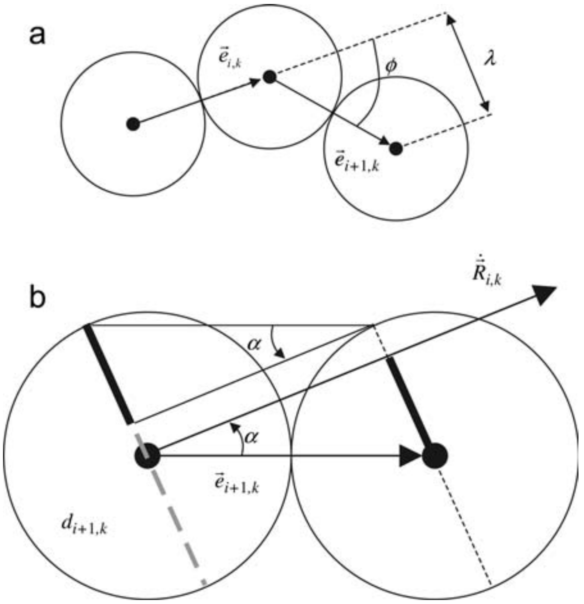

FIGURE 2 Geometrical considerations for establishing the local bending (*a*) and the effective radius of a sphere (*b*). The local bending λ induced by a time-delayed dynamics can be easily computed in terms of the product between the vectors $\vec{e}_{i+1,k}(t)$ and $\vec{e}_{i,k}(t)$ (see text). We include the effect of the local conformation (shape) of cilia by means of an effective radius, $a_{i,k}(t)$, that accounts for the portion of a sphere that is covered by its nearest neighbors with respect to its direction of motion. In this figure we show for sphere i the masking effect due to sphere $i + 1$. We have highlighted the portions of its diameter that are covered and uncovered by means of dashed and solid lines, respectively.

Finally, we briefly detail further fluid dynamics considerations that have been taken into account in our modeling approach. First, even though the extraembryonic fluid is known to be a colloidal suspension of proteins, non-Newtonian effects have been omitted since linear response applies at these low velocities. Second, we have disregarded hydrodynamic coupling between cilia and considered that the effect that cilia and/or nodal flow exert on neighboring cilia dynamics can be neglected. We acknowledge that the feedback induced by hydrodynamic coupling has proved to play an important role in some ciliary phenomena such as metachronal coordination in 9+2 cilia. However, in those cases the intercilia distance is smaller than the cilia length. More importantly, there is no experimental evidence indicating that such effects play a role in nodal 9+0 cilia. Video-microscopy images support this fact (Supplementary Material, Movie S2; and see Okada et al. (5)). Finally, the node is a bounded structure in which the fluid circulates and thus, the leftward flow induced by the cilia motion will eventually return back (with a rightward flow). Since we are mainly interested in how the asymmetric leftward flow is created by the motion of cilia, we have left boundary effects out of our description.

FLUID FLOW INDUCED BY A CILIUM

The formation of an asymmetric leftward flow within the node can be readily analyzed in our proposed modeling framework based on a two-phase cilia dynamics. Since nonplanar two-phase beating nodal cilia bend during the recovery stroke, the effect of conformational changes then comes into play: the effective area exposed to the fluid by the cilia is reduced and therefore so does the velocity transmitted to the fluid (23). As a result a net thrust per revolution is impelled to the fluid and an asymmetric flow may arise (23). It this section we explore the fluid flow dynamics induced by a single cilium to fully characterize the proposed mechanism. To this end, we first briefly analyze a simplified and revealing scenario.

We can reduce the complexity of our model by using the most basic description of a cilium that captures all the dynamics of a three-dimensional beating using only two moving spheres attached to the static floor sphere at the base of the cilium. Thus, we have studied the flow induced by such a cilium by computing the average of the velocity field over a period of motion at different points in space according to

$$\vec{U}(\vec{r}) = \frac{1}{T}\int_0^{\mathrm{T}} \vec{u}_1(\vec{r}, \{\vec{R}_{\mathrm{i,1}}\}, t)dt.$$

The flow is computed at the points $x \in \{-60a, 0, 60a\}$, $y \in \{-60a, 0, 60a\}$ (Fig. 3). The study indicates that a two-phase motion of cilia is, in effect, necessary for inducing a systematic directional flow. If the cilium rotates as a rigid rod (it does not bend) around an axis posteriorly tilted, the flow is leftward on top of the cilium but not all over the space (Fig. 3 *a*). In contrast, if the cilium is straight (power stroke) when moving toward the left and it is bent (recovery stroke) when moving, more slowly, toward the right ($\theta = 3\pi/2$), a net leftward flow arises (Fig. 3 *b*).

Taking into account the latter and returning to the analysis of our model in terms of a complete description of a cilium (16 moving spheres), we have first obtained numerically the trajectory of the tip of a cilium performing a nonplanar beating around an axis tilted to the posterior ($\Theta \approx 40°$) with frequency $f \approx 10$ Hz and apex angle $\Psi \approx 40°$, which are the parameter values characterizing the dynamics of cilia in the mouse node (see Materials and Methods and Okada et al. (5)). We include the time-dependent bending of cilia, by choosing a value of the time delay that leads to the experimentally measured ratio between angular speeds ($\dot{\xi}_{\mathrm{rec}}/\dot{\xi}_{\mathrm{pow}} \approx 0.6 - 0.7$). The projection of the numerically computed trajectory of the tip of the cilium onto the (x-y) plane for these parameter values perfectly fits the experimental data concerning the motion of cilia (Fig. 4 *a*, and Supplementary Material, Movie S1; and see Okada et al. (5)). We have then computed the trajectory of beads embedded in the flow created by this cilium. The beads perform a closed trajectory, moving faster above the cilium than below it. If the bending of the cilium is larger and the recovery stoke becomes slower, the beads become displaced to the left along time (Fig. 4 *b*). In contrast, if the cilium only rotates, without beating (bending), around an axis tilted to the posterior, the beads perform a closed circular trajectory with the same speed above and below the cilium (Fig. 4 *c*).

Our results show that a cilium moving with a two-phase beating dynamics is able to induce an asymmetric flow, which is faster above the cilia than close to the cell surface, in agreement with the fluid flow dynamics described for a 9+2 cilium in paramecium (23). For strong asymmetric two-phase beating dynamics, the fluid flow induced by a single cilium becomes leftward.

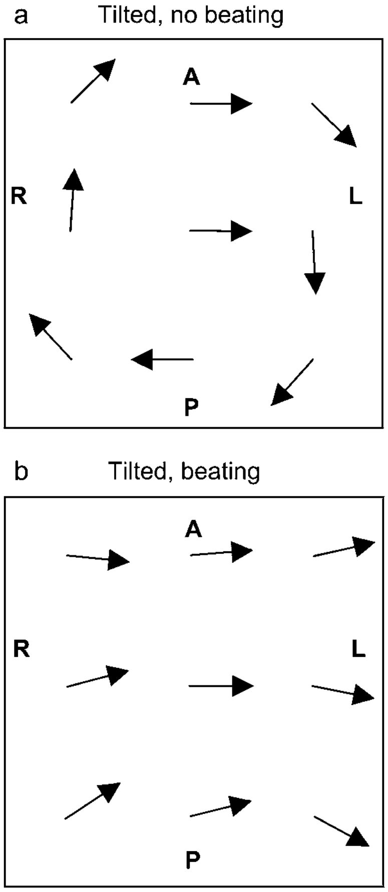

FIGURE 3 Results for the time-averaged flow induced by one cilium at different points (x,y) in the plane $z = 2L$. The base of the cilium is located at the center of the field (x,y,z) = (0,0,0) and its motion is around an axis tilted to the posterior ($\Theta = 0.22\pi \approx 40°$) with apex angle $\Psi = 0.22\pi \approx 40°$. The length of the cilium is $L = 4a$ ($n = 2$). Vectors have been scaled to the same magnitude. (*a*) If the cilium rotates along a posteriorly tilted axis without bending ($\tau_{\mathrm{b}} = 0$), no systematic leftward flow is induced. (*b*) A net leftward flow is induced if the cilium performs a nonplanar beating motion around an axis tilted to the posterior with power stroke for leftward motion ($\tau_{\mathrm{b}} = 2\pi/\omega$, $\theta = 3\pi/2$).

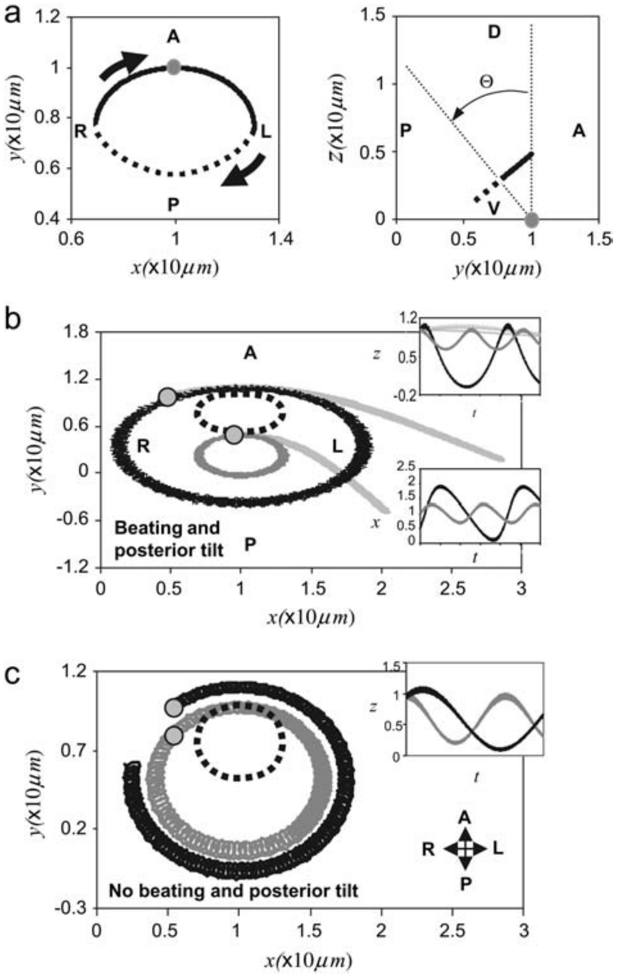

FIGURE 4 Numerical results for the motion of a cilium and beads embedded in the flow generated by a single cilium for different ciliary dynamics. (*a*) Trajectory of the tip of a cilium tilted to the posterior with a nonplanar beating motion with power stroke toward the left (*full line*) and recovery stroke (*dotted line*) toward the right ($n = 16$, $\theta = 3\pi/2$, $\tau_b = 0.5\pi/\omega$, $\Psi = \Theta = 0.22\pi \approx 40°$). The base of the cilium is indicated by the shaded circle. (*b* and *c*) Dynamics of beads. Shaded circles show the initial position of beads. The dotted lines corresponds to the projection of the trajectory of the tip of the cilium. The motion of beads is tracked over the entire space during more than 300 periods of beating or rotation and projected onto the (*x-y*) plane. (*b*) The beads (*solid*, *dark shading*) embedded in the flow created by a cilium with a nonplanar beating resembling nodal cilia ($\tau_b = 0.5\pi/\omega$, $\Psi = \Theta = 0.22\pi \approx 40°$, $\theta = 3\pi/2$) move faster on top of the cilium than close to the cell surface. The beads (*light shading*) embedded in the flow created by a cilium with a stronger bending and a slower recovery stroke move leftward ($\tau_b = 2\pi/\omega$, $\Psi = \Theta = 0.22\pi \approx 40°$, $\theta = 3\pi/2$). (*c*) The beads embedded in the flow induced by a cilium that rotates as a rigid rod ($\tau_b = 0$) around an axis tilted to the posterior ($\Psi = \Theta = 0.22\pi \approx 40°$) rotate with uniform speed.

MOTION OF PASSIVE TRACERS IN THE MURINE NODE

We now focus on the flow induced by many of these beating cilia distributed on a pearlike shape as in the murine node. As in experimental assays, we have tracked the trajectory of several beads distributed along the node and set initially at $z = 5–7\ \mu$m on top of the cell surface (base of the node). Cilia are nonsynchronized. We have checked that cilia synchronization induces no appreciable effect in the behavior of the fluid flow. Our in silico studies show that, for the bending and beating dynamics of nodal cilia (Fig. 4 *a*, and Supplementary Material, Movies S1 and S2), the beads move toward the left performing some swirls (Fig. 5 *a*, and Supplementary Materials, Movie S3). The motion of these beads is in perfect agreement with the experimental data. The average speed of several beads distributed over the entire node at 5 μm above the cell surface is $\langle u_x \rangle = 14 \pm 6\ \mu$m/s (leftward, Fig. 5 *b*), which is in the range of fluid flow speeds reported in experimental studies (2,3,5).

In addition, our model unveils how the flow depends on different parameters of the ciliary dynamics. In Fig. 5 *c* we show for the *wt* situation the dependence of the flow on the asymmetry between the power and recovery strokes by keeping the same angular velocity (that is, depending on the stiffness of cilia). As the angular speed of the recovery stroke decreases with respect to the power stroke, the leftward fluid flow becomes faster. In Fig. 5 *d* we show that larger intercilia distances also reduce the fluid flow speed. Other in silico experiments show that the leftward flow is slower if the frequency of motion is lower, cilia are shorter, the apical angle is smaller, and/or the tilting angle is reduced.

MOTION OF PASSIVE TRACERS IN THE *INV* MUTANT NODE

The mechanism proposed herein help us to understand the dynamics of fluid flow in the mouse *inv* mutant. The *inv* homozygous mutants exhibit complete L/R reversal (49). Surprisingly, in *inv* mutants a leftward flow is also registered, and the average angular frequency of cilia is equivalent to that in *wt*. However, the flow velocity is slower than in *wt* phenotypes and the beads trajectories are less directional. We have hypothesized that cilia dynamics appears due to a combined effect of internal and external mechanisms such that the power stroke occurs when less viscous resistance is found by the cilia, i.e., when cilia are moving far from the cell surface. Therefore, anteriorly tilted clockwise rotating cilia would perform their power stroke when moving rightwards, generating a net rightward thrust per revolution. Therefore, we can conjecture that the *inv* mutants anomaly specifies the tilting axis in the sense that a broad distribution of angles holds (that is, in which some cilia are tilted toward the anterior, but with an overall bias to the posterior). Such a hypothesis is, in fact, in agreement with recent experimental results that also show a fraction of cilia are immobile (5). In Fig. 6, and according to recent experimental data, we show a particular case where 50% or the cilia (randomly chosen) are immobile and 20% (randomly chosen) are anteriorly tilted, performing a reversed beating with power stroke toward the right. As expected, our in silico experiments show that, in that

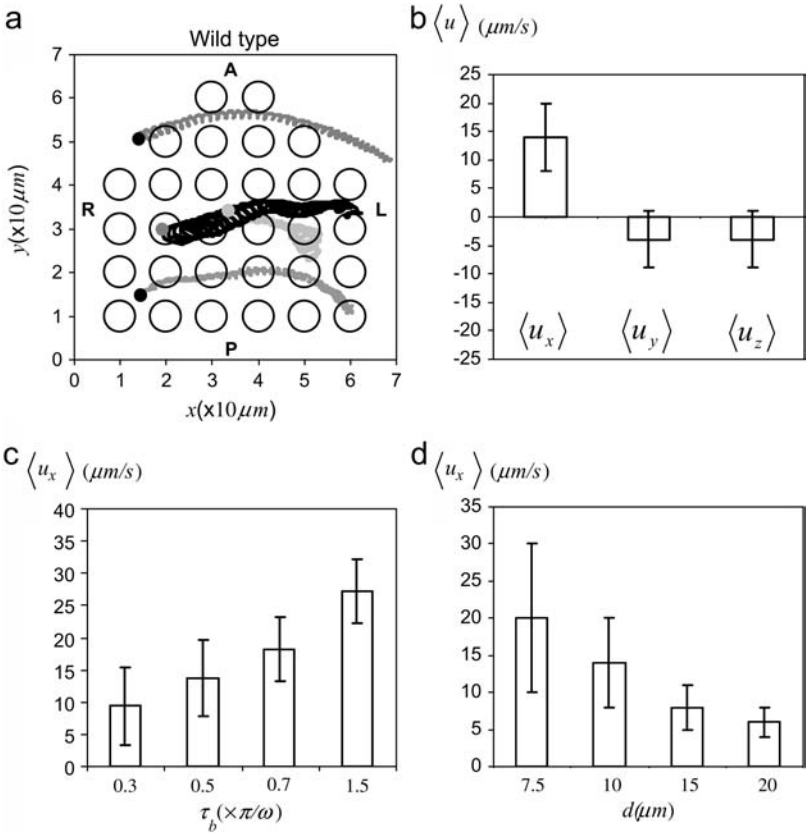

FIGURE 5 Numerical results for the motion of beads and the flow in the murine node. (*a*) Motion of beads embedded in *wt* embryos with beating cilia. The beads are tracked during 60 periods of beating. Dots indicate the initial positions of the beads ($z = 5$ μm). All cilia are posteriorly tilted with their bases located at the center of the circles. The bar stands for the statistical deviation. Anterior (*A*), posterior (*P*), left (*L*), and right (*R*) sides are indicated. (*b*) Average fluid flow velocities for *wt* embryos along the three anatomical axis. (*c–d*) Numerical results for the leftward flow $\langle u_x \rangle$ for different ciliary dynamics and distances between cilia. (*c*) Leftward flow for different bending properties (different time delays t_b). If t_b increases, cilia are more bent and move more slowly during the recovery stroke inducing a faster leftward flow. (*d*) Leftward flow for several distances *d* between cilia. The leftward flow is slower for larger distances between cilia. In both figures, parameter values are $\Psi = \Theta = 0.22\pi \approx 40°$, $\theta = 3\pi/2$, $f = 10$ Hz, $a = 150$ nm, and $n = 16$. The bars correspond to the standard deviation *s*. (*a*, *b*, and *d*) $\tau_b = 0.5\pi/\omega$.

case, the motion of the beads is slower. The flow velocity then reads $<u_x> = 2 \pm 4$ μm/s (leftward), and the trajectories are more erratic than in *wt* embryos (Fig. 6, and Supplementary Material, Movie S3). Other cilia arrangements, keeping the same anomalous distribution of tilting angles, provide an equivalent value of the flow velocity. Importantly, our analysis of cilia dynamics in *inv*/*inv* embryos confirms that a set of cilia is tilted anteriorly and that, in that case, they present a reversed beating—i.e., the power stroke is performed when moving rightwards (Fig. 6, *c* and *d*; and see Okada et al. (5)).

DISCUSSION

The nonplanar dynamics of the cilia that corresponds to our model is characterized by a two-phase nonplanar beating motion in which the cilium moves quickly, rigidly, and vertically toward the left during the power stroke. The return rightward motion, during the recovery stroke, is slower, and the cilium moves close to the cell surface and bends. This nonplanar beating motion is supported by the observed trajectories of the tip of the cilium, as well as by the nonconstant frequency of rotation measured from fast video-recording of the ciliary motion. Thus, by means of polymer hydrodynamics modeling, we show that this motion of cilia (which we propose results from an effective combined effect of viscous interaction between cilia and the cell surfaces and intraciliary dynamics) leads to the emergence of the asymmetric leftward flow. Our modeling approach for describing the dynamics and the shape of a cilium allows for the computation of the time-dependent fluid flow induced by the motion of many moving cilia. Importantly, the effect of the bending of the cilium on the fluid flow is taken into account. In addition, we have set the equation of motion describing the dynamics of a spherical particle, such as a fluorescent bead embedded in the flow. We have also been able to shed some light on the dynamics of the *inv* mutants. By hypothesizing that anteriorly tilted cilia with a clockwise motion will perform the power stroke when moving vertically far from the cell surface and, thus, in a rightward direction, we have been able to numerically obtain the features of the observed flow in *inv* mutant embryos. Finally, our theoretical approach helps to elucidate how the flow depends on different parameters. Hence, by increasing the distance among cilia in our in silico experiments the velocity of the flow is reduced. The same happens when the motions of the power and recovery strokes are more similar and cilia are stiffer. These observations might shed light on recent experimental results on ciliary and fluid flow dynamics for other vertebrate species (5).

Summarizing, we have presented an approximated but powerful modeling framework that provides a platform for understanding the essential biological features of ciliary motion and that accounts for the asymmetry of the fluid flow in the murine node and consequently for the L/R axis

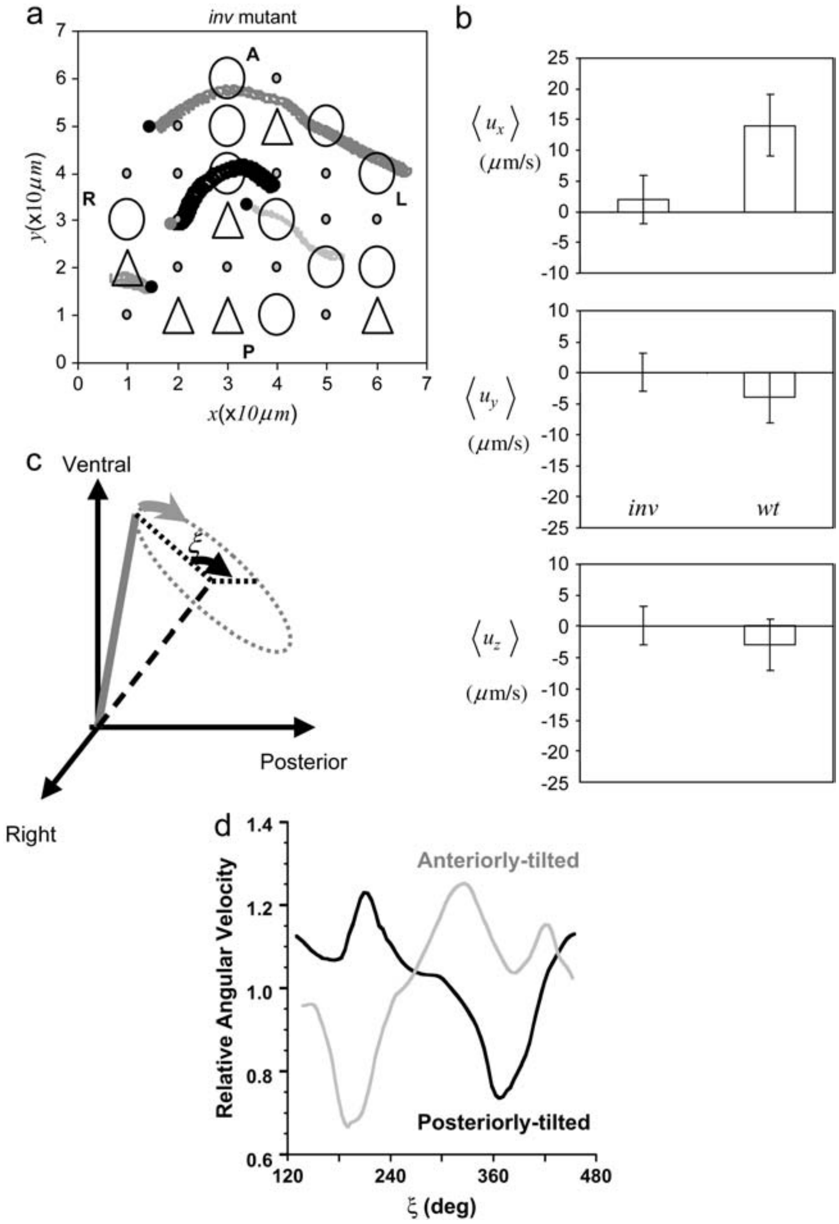

FIGURE 6 In silico and in vivo results for the *inv* mutant. (*a*) In silico motion of beads embedded in a node with 20% of cilia anteriorly tilted (*triangles*) and thus performing a rightward power stroke. In addition, 50% of the cilia are immobile (*small circles*). (*b*) Average fluid flow velocities for *wt* and *inv* mutant embryos along the three anatomical axes. The bar stands for the statistical deviation. (*c*) Angular phase ξ of cilia moving clockwise around a posteriorly tilted axis. The angular speed is computed as the first derivative over time of ξ. (*d*) Numerical analysis of in vivo video-microscopy data depicting the angular velocity of the tip of cilia in *inv*/*inv* mutants as a function of the angular position for two representative cases (see Okada et al. (5) for further details). Anteriorly tilted cilia perform a reversed dynamics with respect to cilia that are posteriorly tilted. Parameter values for in silico experiments are $\theta = 3\pi/2$ and $\Theta = 0.22\pi \approx 40°$ (*circles*), $\theta = \pi/2$, and $\Theta = -0.22\pi \approx -40°$ (*triangles*), $\Psi = 0.22\pi \approx 40°, f = 10$ Hz, $a = 150$ nm, $\tau_b = 0.5\ \pi/\omega$, and $n = 16$.

specification. Thus, an anteroposterior asymmetry (posterior tilting) coupled to a dorsoventral asymmetry (ventral protrusion of clockwise rotating cilia) elicits a L/R symmetry-breaking event in the ciliary dynamics that, in an early stage, is collectively translated to the entire ciliated organ by the fluid flow.

SUPPLEMENTARY MATERIAL

An online supplement to this article can be found by visiting BJ Online at http://www.biophysj.org.

We thank Dr. K. Lindenberg, Dr. P. Español, Dr. J. Isern-Fontanet, Dr. C. Kintner, Dr. G. Sternik, Dr. M. Morita, Dr. A. Raya, and the reviewers for fruitful comments and insights. We also thank Sen Takeda and Yosuke Tanaka from the Hirokawa lab for their help.

J.B. acknowledges support by the La Jolla Interfaces in Science Interdisciplinary Program funded through the generosity of the Burroughs Wellcome Fund. M.I. acknowledges support by the Fulbright Program and Generalitat of Catalunya. This work was supported by grants from the Human Frontier Science Program, the National Institutes of Health, the G. Harold and Leila Y. Mathers Charitable Foundation, the Banco Bilbao Vizcaya Argentaria Foundation, and by a Center of Excellence Grant-in-Aid from the Ministry of Education, Culture, Sports, Science and Technology of Japan (N.H.).

REFERENCES

1. Gilbert, S. 2003. Developmental Biology, 7th Ed. Sinauer, Sunderland, MA.
2. Nonaka, S., Y. Tanaka, Y. Okada, S. Takeda, A. Harada, Y. Kanai, M. Kido, and N. Hirokawa. 1998. Randomization of left-right asymmetry

due to loss of nodal cilia generating leftward flow of extraembryonic fluid in mice lacking KIF3B motor protein. *Cell*. 95:829–837.

3. Okada, Y., S. Nonaka, Y. Tanaka, Y. Saijoh, H. Hamada, and N. Hirokawa. 1999. Abnormal nodal flow precedes situs inversus in *iv* and *inv* mice. *Mol. Cell*. 4:459–468.
4. Essner, J. J., K. J. Vogan, M. K. Wagner, C. J. Tabin, H. J. Yost, and M. Brueckner. 2002. Conserved function for embryonic nodal cilia. *Nature*. 418:37–38.
5. Okada, Y., S. Takeda, Y. Tanaka, J. C. Izpisúa-Belmonte, and N. Hirokawa. 2005. Mechanism of nodal flow: a conserved symmetry-breaking event in left-right axis determination. *Cell*. 121:633–644.
6. Takeda, S., Y. Yonekawa, Y. Tanaka, Y. Okada, S. Nonaka, and N. Hirokawa. 1999. Left-right asymmetry and kinesin superfamily protein KIF3A: new insights in determination of laterality and mesoderm induction by KIF3A−/− mice analysis. *J. Cell Biol.* 145:825–836.
7. Marszalek, J. R., P. Ruiz-Lozano, E. Roberts, K. R. Chien, and L. S. Goldstein. 1999. Situs inversus and embryonic ciliary morphogenesis defects in mouse mutants lacking the KIF3A subunit of kinesin-II. *Proc. Natl. Acad. Sci. USA*. 96:5043–5048.
8. Nonaka, S., H. Shiratori, Y. Saijoh, and H. Hamada. 2002. Determination of left-right patterning of the mouse embryo by artificial nodal flow. *Nature*. 418:96–99.
9. Kawakami, Y., A. Raya, R. M. Raya, C. Rodriguez-Esteban, and J. C. Belmonte. 2005. Retinoic acid signalling links left-right asymmetric patterning and bilaterally symmetric somitogenesis in the zebrafish embryo. *Nature*. 435:165–171.
10. Tabin, C. J., and K. J. Vogan. 2003. A two-cilia model for vertebrate left-right axis specification. *Genes Dev.* 17:1–6.
11. McGrath, J., S. Somlo, S. Makova, X. Tian, and M. Brueckner. 2003. Two populations of node monocilia initiate left-right asymmetry in the mouse. *Cell*. 114:61–73.
12. Meinhardt, H. 2001. Organizer and axes formation as a self-organizing process. *Int. J. Dev. Biol.* 45:177–188.
13. Raya, A., Y. Kawakami, C. Rodriguez-Esteban, M. Ibañes, D. Rasskin-Gutman, J. Rodriguez-Leon, D. Buscher, J. A. Feijo, and J. C. Izpisúa Belmonte. 2004. Notch activity acts as a sensor for extracellular calcium during vertebrate left-right determination. *Nature*. 427:121–128.
14. Rasskin-Gutman, D., and J. C. Izpisúa-Belmonte. 2004. Theoretical morphology of developmental asymmetries. *Bioessays*. 26:405–412.
15. Gueron, S., and K. Levit-Gurevich. 2001. A three-dimensional model for ciliary motion based on the internal 9+2 structure. *Proc. R. Soc. Lond. B. Biol. Sci.* 268:599–607.
16. Brokaw, C. J. 2002. Computer simulation of flagellar movement VIII: coordination of dynein by local curvature control can generate helical bending waves. *Cell Motil. Cytoskeleton*. 53:103–124.
17. Dillon, R. H., and L. J. Fauci. 2000. An integrative model of internal axoneme mechanics and external fluid dynamics in ciliary beating. *J. Theor. Biol.* 207:415–430.
18. Lenz, P., J. F. Joanny, F. Julicher, and J. Prost. 2003. Membranes with rotating motors. *Phys. Rev. Lett.* 91:108104-1–108104-4.
19. Brokaw, C. J. 2005. Computer simulation of flagellar movement IX. Oscillation and symmetry breaking in a model for short flagella and nodal cilia. *Cell Motil. Cytoskeleton*. 60:35–47.
20. Cartwright, J. H., O. Piro, and I. Tuval. 2004. Fluid-dynamical basis of the embryonic development of left-right asymmetry in vertebrates. *Proc. Natl. Acad. Sci. USA*. 101:7234–7239.
21. Purcell, E. M. 1977. Life at low Reynolds number. *Am. J. Phys.* 45: 3–11.
22. Vogan, K. J., and C. J. Tabin. 1999. A new spin on handed asymmetry. *Nature*. 397:297–298.
23. Blake, J. 1974. Hydrodynamic calculations on the movements of cilia and flagella. I. Paramecium. *J. Theor. Biol.* 45:183–203.
24. Sleigh, M. A. 1974. Cilia and Flagella. Academic Press, New York.
25. Wheatley, D. 2004. Primary cilia: new perspectives. *Cell Biol. Int.* 28: 75–77.
26. Woolley, D. M. 1998. Studies on the eel sperm flagellum. III. Vibratile motility and rotatory bending. *Cell Motil. Cytoskeleton.* 39:246–255.
27. Wakabayashi, K., Y. Yagi, and R. Kamiya. 1997. Ca^{2+}-dependent waveform conversion in the flagellar axoneme of *Chlamydomonas* mutants lacking the central-pair/radial spoke system. *Cell Motil. Cytoskeleton.* 38:22–28.
28. Woolley, D. M., and G. G. Vernon. 2001. A study of helical and planar waves on sea urchin sperm flagella, with a theory of how they are generated. *J. Exp. Biol.* 204:1333–1345.
29. Ishijima, S., K. Sekiguchi, and Y. Hiramoto. 1988. Comparative study of the beat patterns of American and Asian horseshoe crab sperm: evidence for a role of the central pair complex in forming planar waveforms in flagella. *Cell Motil. Cytoskeleton.* 9:264–270.
30. De la Torre, J., and V. A. Bloomfield. 1977. Hydrodynamic theory of swimming of flagellated microorganism. *Biophys. J.* 20:49–67.
31. Gibbons, I. R. 1981. Cilia and flagella in eukaryotes. *J. Cell Biol.* 91: 107s–124s.
32. Alberts, B., A. Johnson, J. Lewis, M. Raff, K. Roberts, and P. Walter. 2002. Molecular Biology of the Cell, 4th Ed. Garland Science, New York.
33. Kartagener, M., and A. Horlacher, A. 1936. *Situs viscerum inversus* and nasal polyposis in a family case study of Bronchiectasia. *Beitr. Klin. Tuberk.* 87:331–333.
34. Afzelius, B. A. 1976. A human syndrome caused by immobile cilia. *Science.* 193:317–319.
35. Wemmer, K. A., and W. F. Marshall. 2004. Flagellar motility: all pull together. *Curr. Biol.* 14:R992–R993.
36. Morita, Y., and C. Shingyoji. 2004. Effects of imposed bending on microtubule sliding in sperm flagella. *Curr. Biol.* 14:2113–2118.
37. Nelson, P. C. 2004. Biological Physics: Energy, Information, Life, 1st Ed. Freeman, New York.
38. Anselmi, C., P. DeSantis, and A. Scipioni. 2005. Nanoscale mechanical and dynamical properties of DNA single molecules. *Biophys. Chem.* 113:209–221.
39. Gittes, F., B. Mickey, J. Nettleton, and J. Howard. 1993. Flexural rigidity of microtubules and actin filaments measured from thermal fluctuations in shape. *J. Cell Biol.* 120:923–934.
40. Gueron, S., and K. Levit-Gurevich. 1999. Energetic considerations of ciliary beating and the advantage of metachronal coordination. *Proc. Natl. Acad. Sci. USA.* 96:12240–12245.
41. Okuno, M., D. J. Asai, K. Ogawa, and C. J. Brokaw. 1981. Effects of antibodies against dynein and tubulin on the stiffness of flagellar axonemes. *J. Cell Biol.* 91:689–694.
42. Feynman, R. P. 1964. The Feynman Lectures in Physics, Vol. II. Addison-Wesley, Reading, MA.
43. Huner, B., and R. G. Hussey. 1977. Cylinder drag at low Reynolds number. *Phys. Fluids.* 20:1211–1218.
44. Maxey, M. R., and J. J. Riley. 1983. Equation of motion for a small rigid sphere in a nonuniform flow. *Phys. Fluids.* 26:883–889.
45. Landau, L. D., and E. M. Lifshitz. 1959. Hydrodynamics. Pergamon, New York.
46. Kirkwood, J. G., and J. Riseman. 1948. The intrinsic viscosities and diffusion constants of flexible macromolecules in solution. *J. Chem. Phys.* 16:565–573.
47. Doi, M., and S. F. Edwards. 1986. The Theory of Polymer Dynamics. Clarendon, Oxford.
48. Gray, J., and G. J. Hancock. 1955. The propulsion of sea-urchin spermatozoa. *J. Exp. Biol.* 32:802–814.
49. Yokohama, T., N. G. Copeland, N. A. Jenkins, C. A. Montgomery, F. F. Elder, and P. A. Overbeek. 1993. Reversal of left-right asymmetry: a situs inversus mutation. *Science.* 260:679–682.